Anisotropy, orbital order, and colossal electroresistance in untwinned $La_{0.9}Sr_{0.1}MnO_3$ single crystals

A. de Andrés,[1,*] N. Biškup,[1] M. García-Hernández,[1] and Y. M. Mukovskii[2]
[1]*Instituto de Ciencia de Materiales de Madrid, Consejo Superior de Investigaciones Científicas, Cantoblanco, E-28049 Madrid, Spain*
[2]*Moscow State Steel and Alloys Institute, Leninskii prospekt 4, Moscow 119049, Russia*
(Received 17 June 2008; revised manuscript received 25 November 2008; published 28 January 2009)

A magnetic and electric transport study of twinned and untwinned $La_{1-x}Sr_xMnO_3$ single crystals, with Sr content corresponding to a vertical phase diagram boundary ($x \approx 0.1$), is presented. The phases distinctive of both phase diagram sides are consecutively detected. All magnetic, transport, and electroresistance properties are found to be anisotropic. Below the ferromagnetic ordering, $T_{C1}=143$ K, we have detected a second magnetic transition ($T_{C2}=125$ K) with an easy ferromagnetic direction along the *c* axis and antiferromagnetic order (AF) along the *a* and/or *b* axes. The glassylike behavior of the ferromagnetic phase disappears when the AF correlations become long ranged. The magnetocrystalline anisotropy remains below the orbital ordering transition ($T_{C3}=73$ K) with a strong anomaly in the coercive field at 30 K. The system is insulating at any temperature with different activation energies depending on the direction of the current below T_{C1}. The observed magnetic anisotropy below T_{C2} is consistent with a homogeneous picture of the system as the ordered orbital polaron lattice proposed for the $x=0.125$ compound. Typical negative magnetoresistance (MR) for single crystals is detected, except at temperatures between both magnetic transitions, $T_{C3}<T<T_{C2}$, where the positive MR is due to the promotion of the orbital order. Applied magnetic fields up to 14 T could not remove the orbital order while low-current densities ($j=10^{-8}$ A/cm^2 at $T=20$ K), when applied along the AF axes, are able to destroy the orbital order and delocalize the carriers inducing a metalliclike conductivity and reducing the resistivity by a factor of up to 10^7. The observation of anisotropic electroresistance (ER) both in continuous and pulsed regimes, consistent with magnetic and transport anisotropies, as well as the low-current densities necessary to induce the phase transition, excludes Joule heating as the origin of the discontinuous high to low resistance transitions in these single crystals.

DOI: 10.1103/PhysRevB.79.014437 PACS number(s): 75.47.Lx

I. INTRODUCTION

Mixed valence manganites $R_{1-x}A_xMnO_3$ (R=trivalent La or rare earth, A=divalent Ca, Sr, or Ba, $0<x<1$) are widely recognized to be the role model for systems of strongly correlated electrons due to their intercoupling of spin, charge, and orbital degrees of freedom. Small changes in divalent doping concentration "x" (fraction of Mn^{4+}) can lead to dramatic changes in the magnetic and transport properties as well as in the crystalline structure, orbital order, and phase segregation.[1] Among these compounds, lightly doped $La_{1-x}Sr_xMnO_3$ ($x<0.15$) are particularly interesting since they present a complex phase diagram[2] which includes almost all electronic, structural, orbital, and magnetic phases of manganites [Fig. 1(a)]. Around $x=0.1$ (the exact limit is still not well defined) a vertical phase boundary separates the regime for $x<0.1$ compounds, which are very similar to the cooperatively Jahn-Teller (JT) distorted *A* type antiferromagnetic (AF) insulating undoped $LaMnO_3$, to that, more complicated, for $x>0.1$ with two structural phase transitions related to different orbital orders, a complex magnetic scenario and several regimes for electronic conduction. Almost all available techniques, more or less sophisticated, have been used to obtain a picture of the different phases, mainly focused on the $x=1/8$ composition. The different techniques gave complementary information but their conclusions did not always point to the same direction maintaining some uncertainty in several fundamental aspects. The presence of different kinds of electronic[3] and/or chemical inhomogeneities,[4] glassy behavior,[2] Griffiths phase,[5] or nanophase segregation[6] in the different temperature ranges have been invoked to explain the observations. But also homogeneous pictures of the low-temperature phases have been reported.[7,8] In summary, the different phases of the compounds in the range $0.1 \leq x \leq 0175$ are still under debate.

The title compound $La_{0.9}Sr_{0.1}MnO_3$ is situated at the border between the canted antiferromagnetic (CAF) and ferromagnetic insulator (FMI) phases of the x-T phase diagram; therefore, its actual composition is especially critical. The three phase transition temperatures reported by different authors for this nominal composition present a large dispersion [see Figs. 1(a) and 1(b)] demonstrating the intrinsic difficulty to study this compound. $La_{0.9}Sr_{0.1}MnO_3$ structure at room temperature has been described either by the orthorhombic *Pbnm* or by the monoclinic $P2_1/c$ space groups.[9] Below the high-temperature structural transition (T_{JT}), the pseudocubic orbital disordered phase transforms either in the orthorhombic *Pbnm* or monoclinic structures depending on x, both with cooperatively Jahn-Teller distorted octahedra and orbital order.[10] This transition temperature T_{JT} is the most sensitive to x [Fig. 1(a)]. Cox *et al.*[9] located the structural phase boundary at $x=0.11$ but their measured T_{JT} for the $x=0.1$ compound is 435 K, well above that reported by other authors (around 320 K). In our case also, T_{JT} is in the 340 K range and an orbital reordering temperature (T_{OO}) is detected below the magnetic order temperature (T_C); therefore we locate our crystals rather on the right side of the phase diagram.

 ©2009 The American Physical Society

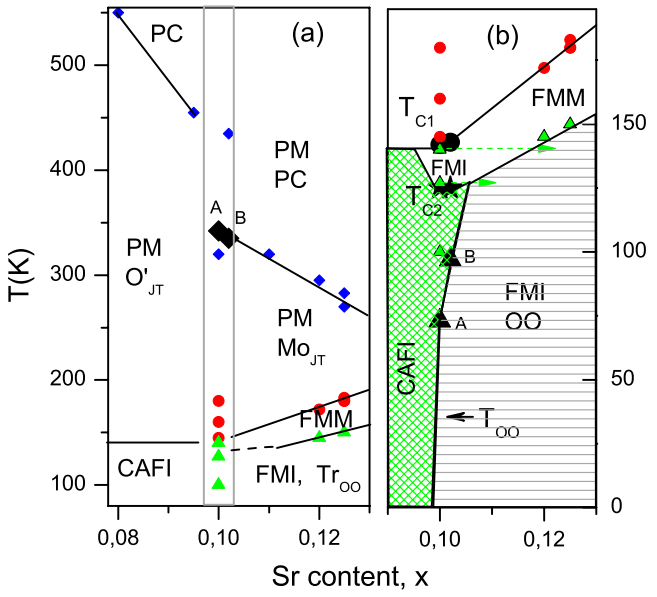

FIG. 1. (Color online) (a) Phase diagram of $La_{0.9}Sr_{0.1}MnO_3$ around the vertical boundary at $x=0.1$. Rhombi: structural transition T_{JT} from pseudocubic (PC) to orthorhombic JT distorted structure (O'_{JT}) for $x<0.1$, and to monoclinic JT distorted (Mo_{JT}) for $x>0.1$. Circles: T_C, triangles: T_{OO}. Small colored symbols correspond to data from Refs. 3, 5, 6, 9, 10, and 15 and large black symbols to the samples A and B (see text). (b) Low-temperature range around $x=0.1$ with the proposed FMI, canted antiferromagnetic insulating (CAFI), and FMIOO regions for $x\approx 0.1$. The stars represent the ferromagnetic to CAFI transition.

Above T_C, for $0.07<x<0.16$, a Griffiths phase has been detected, where FM entities coexist in the PM phase due to the quenched disorder of bonds related to the presence of Mn^{4+} in the cooperatively JT distorted structure.[5] In the $x=0.125$ compound, the easy axis for these FM clusters would lie in the *ab* plane of the *Pbnm* structure. For $x\geq 0.1$, the ferromagnetic order above the orbital phase transition (T_{OO}) has also been shown to be nonuniform, described either as a spin glass[2] or as a nonuniform regime with hole rich metallic walls separating hole deficient insulating regions with "no resemblance to spin or cluster glass."[3] By fitting electron-paramagnetic-resonance data, Rozenberg *et al.*[4] concluded that Sr ions are not uniformly distributed as a result of the crystal-growth method producing an intrinsic inhomogeneity of the samples.

Below the T_{OO} transition a triclinic structure is reported[9] with a different orbital arrangement and a reduced cooperative Jahn-Teller distortion [$x=0.12$ (Ref. 11), $x=1/8$ (Ref. 10)]. Geck *et al.*[7] reported, for $x=1/8$, the formation of a homogeneous orbital polaron lattice (OPL) with a large unit cell $2a_c\times 4b_c\times 4c_c$ (the subscript *c* indicates the pseudocubic cell). The orbital polarons are located around the holes at ordered sites explaining its insulating but ferromagnetic character. An ordered homogeneous phase where Mn and also oxygen charges are modulated in alternating hole rich and hole poor MnO_2 planes[8] is consistent with the OPL. A nonuniform charge distribution scenario below 30 K is deduced from the observation, by nuclear-magnetic resonance, of two Mn subsystems: one similar to a CAF insulator ($x=0.075$) and the other similar to a FM one ($x=0.2$).[12]

There is even more debate on the $x=0.1$ compound. Initially the transition below T_C for $x=0.1$ and 0.125, at around 110 K, was assigned by neutron-diffraction experiments to a canted AF ordering[13] but magnetization data seemed to rather support a transition related to structural changes.[14] Finally there is consensus on the orbital ordering character of this transition but some anomaly in the ac susceptibility was reported in the temperature range between T_C and T_{OO} that was assigned to electronic phase segregation.[6]

In summary, several aspects of the physics of these low doped manganites are still not well established and very specifically of the $x=0.1$ system which lies at a phase diagram boundary. A fundamental point in manganites is whether the inhomogeneity is intrinsic or not: is the observed magnetic inhomogeneity due to electronic phase segregation? Is it supported by chemical or structural intrinsic inhomogeneity? Is it related to the FM-CO phase segregation with or without the assistance of quenched disorder? There is not yet a unique answer that applies for all manganites but it is clear that intrinsic disorder related to the difference in ionic radii at the *A* site does play a fundamental role. The present system ($x=0.1$) is a clear example where diverse results are obtained for an identical nominal composition (Fig. 1) indicating that these results are sample dependent and therefore related in part to extrinsic aspects. This does not exclude intrinsic contributions and a clear purpose has to be to discern between both kinds.

On the other hand, the nature and origin of electroresistance (ER) in manganites are a highly controversial issue. Following the first reports related to the melting of the orbital order by current localization in $Pr_{0.7}Ca_{0.3}MnO_3$,[16] several authors suggested[17–19] that the origin of ER was Joule heating. ER was reported even in compounds without charge or orbital order, $Pr_{0.8}Ca_{0.2}MnO_3$,[20] and was interpreted as pure Joule heating on the current paths due to large currents. Reports[18–20] concern polycrystalline samples whose conductivity strongly depends on intergrain transport. In granular manganites, even in the ferromagnetic regime of optimally doped ones, metallic and insulating paths coexist and their ratio is determined by the intergrain connectivity and grains surface.[21] In this situation filamentary conduction does occur and local heating is significantly enhanced. Therefore, polycrystals are not the best systems to study *I-V* nonlinearity. In the last few years there have been also a large number of reports on ER in thin films. But thin films have specific problems related to the large current densities passing through them ($j_{TF}\approx 10^6 j_{SC}$) and the influence of structural distortions due to substrates[22] that make them not easily comparable to bulk systems. Single crystals are definitely the best choice to study intrinsic ER. In single crystals, it was found, for example, that in the FM insulating state of $La_{0.82}Ca_{0.18}MnO_3$ the ER at very small currents ($I<50$ uA) is equivalent to magnetoresistance (MR) (Ref. 23) while ER and MR are not directly related in other compounds.[24,25] In any case, ER is always accompanied and sometimes even dominated by heating. In fact ER observed in Refs.17–20 is always continuous while reports of discontinuous transitions between states with different resistivity cannot be explained only by heating.[24,26] The observation of ER both in continuous and

pulsed applied voltage or current is necessary to discern between Joule heating and intrinsic mechanisms.

In this work we present a comparative study of magnetic and electrical transport properties of single crystals of $La_{0.9}Sr_{0.1}MnO_3$ cut from two different ingots—one with the usual twinning [(100), (010), and (112) domains, *Pbnm* notation] and the other only with (100) and (010) domains—paying special attention to the temperature region between T_C and T_{OO} transitions. We report in bulk samples, evidence of anisotropy in the magnetization as well as in electric conduction and electroresistance. We discuss the different phases of these samples that show an anisotropic magnetic transition between T_C and T_{OO}. We show that below this transition the easy ferromagnetic (FM) axis is along the crystal c axis while AF coupling occurs along the a and/or b axes. Such magnetic anisotropy is reflected in electrical transport and especially pronounced in the case of ER which is observed along the AF axes, while suppressed along the easy FM axis.

II. EXPERIMENTAL

Single crystals of $La_{0.9}Sr_{0.1}MnO_3$ were prepared by the floating zone technique.[27] Samples from two ingots of nominally identical composition were measured. A typical sample is a disk (thickness 1–3 mm) cut perpendicular to the ingot growth axis (ga). In this report we present results from one sample from the first ingot (ϕ=5 mm), labeled as sample A, and another from the second ingot (ϕ=3 mm), labeled B. Magnetic measurements were done in a Quantum Design superconducting quantum interference device (SQUID) (magnetometer) and physical property measurement system (PPMS) with field parallel and perpendicular to the growth axis. Transport measurements were performed in the PPMS and in an Oxford cryostat. Several different models of current sources and voltmeters were used in order to eliminate the possibility of experimental artifacts. At low temperatures, where the resistance diverges ($T<70$ K), I-V curves were taken in constant voltage mode, i.e., measuring current. In the range $70<T<300$ K, dc measurements (in constant current mode and in agreement with the constant voltage mode near 70 K) were accompanied by pulsed measurements (0.5 ms pulses). The electrical contacts were done by gluing four 25 um golden wires with a standard ("Dupont") silver paste.

III. RESULTS AND DISCUSSION

The nominal composition of $La_{0.9}Sr_{0.1}MnO_3$ single crystals is at a boundary in the x-T phase diagram where both structural and magnetic phases, as well as order temperatures, are different. The sharp increase in the magnetization moment per Mn in the x=0.09 to 0.11 range (from $1.2\mu_B$ to $3.9\mu_B$) cannot be explained by a continuous increase of the canted angle.[2] Phase segregation and spin-glass disorder have been used to explain this region of the x-T phase diagram to pass from the A type canted AF order to collinear ferromagnetism, but further work is necessary to study in detail the magnetic and electric transports of this crucial composition. A single crystal with only (100) and (010) domains, which we will call "untwinned" by comparison with the usual twinning, has provided the access to important information on anisotropy.

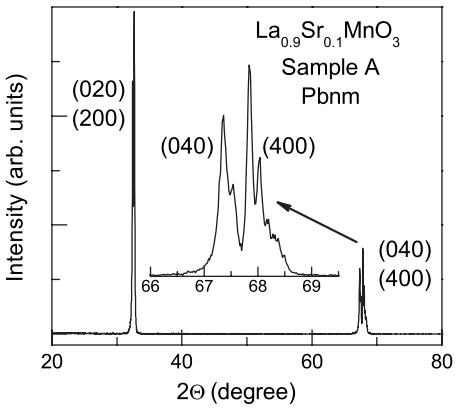

FIG. 2. Diffraction of sample A in Θ-2Θ configuration with the sample surface perpendicular to the scattering plane. (The double peaks are due to the $k_{\alpha 1}$ and $k_{\alpha 2}$ components of the incident Cu radiation.)

We compare the results obtained from two single crystals cut from two ingots, one "untwinned" (sample A) and the other twinned (sample B). Both show identical ferromagnetic order temperature, within 1 K, and different structural Jahn-Teller transition temperatures at 342 K (A) and 335 K (B).

In order to check the twinning and orientation of sample A we have performed a diffraction experiment in a Θ-2Θ configuration with the sample surface perpendicular to the scattering plane. The only detected peaks, for 2Θ between 20 and 80°, correspond to (020), (200), (040), and (400) reflections in the *Pbnm* space group notation (Fig. 2). Previous ω, φ, and χ scans were done to maximize the 2Θ peak intensity in order to find the deviation of the growth axis from the crystallographic axis. The maximum intensity occurs at 6.5° off the expected value from 2Θ. Therefore, the a and the b axes are almost parallel to the ga (in fact deviated 6.5°) and the c axis is nearly perpendicular to it.

In the inset of Fig. 2, a zoom of the (040) and (400) region is shown. The usual twinning for this kind of manganite crystals, with $a \approx b \approx c/\sqrt{2}$, corresponds to the simultaneous presence of crystallographic regions oriented along (100), (010), and (112) (and their opposite vectors) due to the close values of (400), (040), and (224) interplane distances. In polycrystalline samples, while the (112) intensity is very weak, the (224) diffraction intensity [which lies in the (400) and (040) angular region] is ten times that of (040); therefore this region is a good test to check this kind of twinning. Since no significant indication of (224) peaks is detected we can conclude that there is only a twinning between the a and b axes of the *Pbnm* cell but not with (112) (we will call this sample A "untwinned") which usually occurs in this kind of crystals and in fact does occur for sample B.

A. Magnetic anisotropy

Figure 3(a) shows the magnetic susceptibility χ of the untwinned sample A measured at 1000 Oe for magnetic field parallel and perpendicular to the growth axis. Differences

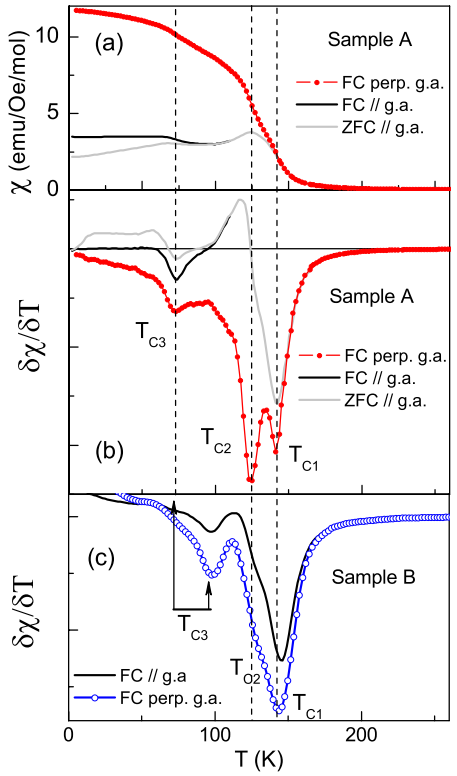

FIG. 3. (Color online) (a) Magnetic susceptibilities χ at 1000 Oe, (b) derivatives $d\chi/dT$ for sample A, and (c) susceptibility derivatives for sample B, in two different field directions parallel and perpendicular to the ga. $T_{C1}=T_C$, $T_{C3}=T_{OO}$, T_{C2}: anisotropic magnetic transition.

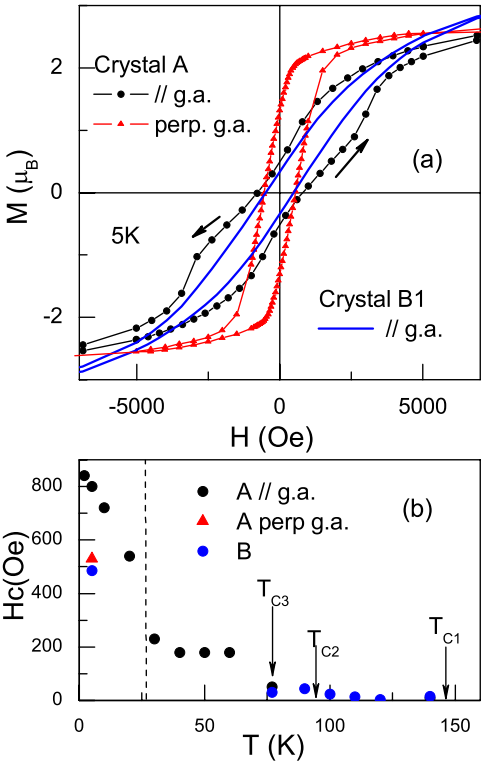

FIG. 4. (Color online) (a) Magnetic cycles at 5 K for the untwinned sample A, with H parallel and perpendicular to the growth axis, and for twinned sample B with $H\|$ga. (b) Dependence of the coercive field H_C with temperature. The dashed line indicates an anomaly at around 30 K.

between the susceptibilities for both measured directions can be observed and are clearly revealed in their derivatives $d\chi/dT$ [Fig. 3(b)]. From these derivatives it is possible to distinguish three transition temperatures: $T_{C1}=142$ K, $T_{C2}=125$ K, and $T_{C3}=73$ K (minima of $d\chi/dT$). T_{C1} corresponds to T_C (circles in Fig. 1) and T_{C3} to the orbital-order transition T_{OO} (triangles in Fig. 1) (we will use T_C and T_{OO} hereafter). T_C and T_{OO} are observed for both field directions. Another feature is detected at T_{C2} which is strongly anisotropic: for $H\|$ga the susceptibility starts to decrease while a new inflection point occurs for $H\perp$ga. This may be interpreted as a magnetic structure where the direction perpendicular to the ga is an easy ferromagnetic axis while antiferromagnetic correlations are established along the ga.

The samples are short cylinders (disks) with different length (L) to diameter (D) ratios, with $L\leq D$ and ga$\|L$; therefore shape anisotropy favors the magnetization perpendicular to the ga.[28] It is not trivial to discern between shape and magnetocrystalline effects since both are acting in the same direction. In fact, the different values of the susceptibility in both directions in Fig. 3 cannot be interpreted only in terms of crystalline anisotropy, but their different evolution with temperature, evidenced in their temperature derivatives, can be. This is confirmed by comparing Fig. 3(b) to the susceptibility derivatives $d\chi/dT$ of the twinned sample B measured in with $H\|$ga and $H\perp$ga [Fig. 3(c)] that, contrary to the A crystal, are almost identical. Since both samples have the same shape, shape anisotropy cannot be the origin of the anisotropy observed in sample A. Thus, below T_{C2}, the easy FM crystalline axis in sample A ($\perp$ga) lies in the plane containing the c axis, while a and/or b are hard axes. Here, the AF component is occurring along the a or b axis and not along the c axis. Thus the anisotropic magnetic structure may be described as a ferromagnetic structure with an AF canting along the a and/or b axes, which differs from the A type AF structure where the AF order is along the c axis. In samples from ingot B it is not possible to clearly detect the anisotropy related to the c axis since any direction contains contributions from the three axes (a, b, and c) through the different crystallographic domains.

It is noted that the magnetic transition temperatures T_C and T_{C2} are very close in all the samples, while T_{OO} shows a large variation: between 73 K for sample A to 97 K for sample B. This indicates that the temperature at which the low-temperature orbital order is established depends critically on very small compositional differences when $x\approx 0.1$ and probably on the particular distribution of Sr in each sample, explaining the discrepancies in the literature for the reported T_{OO} values.

The magnetization loops vs magnetic field of sample A at low temperatures [Fig. 4(a)] show an axial anisotropy also at $T=5$ K. Again, for the applied magnetic field $H\perp$ga the cycle corresponds to a quite standard ferromagnetic behavior and coincides with the FM easy axis. On the contrary, the linear behavior at low fields for $H\|$ga indicates a hard FM or AF axis. The steps in $M(H)$ around 2500 Oe may be the

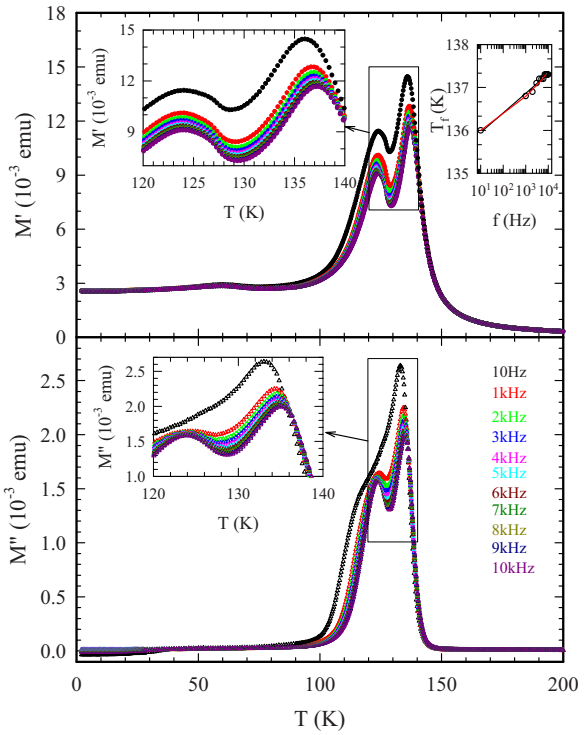

FIG. 5. (Color online) Real and imaginary parts of ac magnetization for sample A with $H \perp$ ga at the indicated frequencies. Left insets show the frequency dependence of T_{C1} and T_{C2} transitions. Upper right inset shows an Arrhenius plot for T_{C1}.

signature of the unpinning of the spins by the external field. It is noted that, even at 5 T the magnetization (between $3.2\mu_B$ and $3.4\mu_B$) is quite below the saturation value expected from Mn collinear spin order ($3.9\mu_B$). Again, the magnetic cycle of the twinned sample B measured with H∥ga [Fig. 4(a)] shows that shape anisotropy does not account for the features observed in the untwinned sample A in the same geometry. The deviation of the zero field cooled (ZFC) curve from the field cooled (FC) [Fig. 3(a)], both measured at 1000 Oe, up to temperatures as high as T_{C2} (125 K) when the coercive field at 77 K is lower than 100 Oe, may also be a consequence of antiferromagnetic coupling. Figure 4(b) shows the dependence of the coercive field measured for samples A and B revealing a clear anomaly around 30 K.

The magnetic order for $T_C > T > T_{OO}$ has been explained through different scenarios: spin-glass-like, canted AF, or phase segregation. Since a magnetic phase transition at T_{C2} occurs in this temperature range, ac susceptibility has been recorded for sample A with $H \perp$ ga to check a possible spin glass or cluster-glass behavior at any of the three critical temperatures (Fig. 5). No evidence of spin-glass-like behavior is detected around T_{C2} or T_{OO} while the temperature of the T_C transition slightly increases (1.5 K) in the measured frequency range. Frequency and field dependences of the T_C transition are observed, contrary to the reported data for a polycrystal with nominal composition $x=0.1$ and T_C around 180 K,[3] pointing to some disorder and magnetic frustration indicating that it corresponds to a spin-glass-like transition as in Ref. 2.

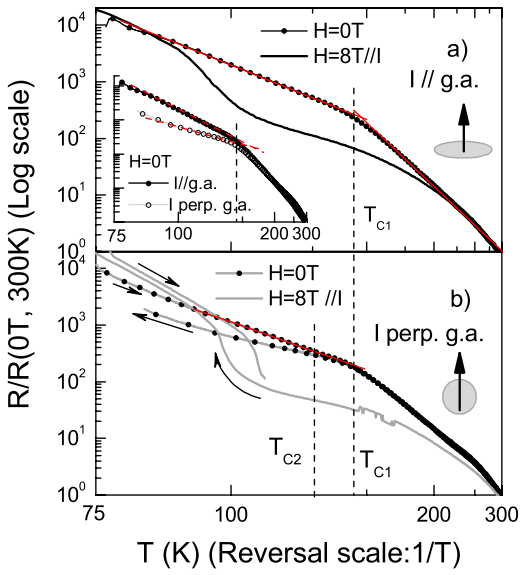

FIG. 6. (Color online) Resistance of sample A for current (a) $I \parallel$ and (b) $\perp$ to ga at $B=0$ T and $B=8$ T. The resistance is normalized to R (300 K, 0 T) values in each direction. Cooling and heating sweeps are shown. Inset compares $H=0$ T curves, both cooling the sample, to evidence the anisotropy.

B. Conductivity anisotropy

In order to evaluate the anisotropy of electric transport surmounting the inevitable large error introduced by the estimation of the geometrical factors, we have normalized the measured resistivity to the R (300 K, 0 T) values in each direction (0.6 Ω for $I \parallel$ga and 6.1 Ω for $I \perp$ ga). In this way we can evaluate the anisotropy at lower temperatures. Figure 6 shows the normalized resistance $R(T)/R$ (0 T, 300 K) of sample A for current $I \parallel$ga [Fig. 6(a)] and $I \perp$ ga [Fig. 6(b)] at $H=0$ T and $H=8$ T maintaining $I \parallel H$. The inset compares the normalized resistances in both directions to $H=0$ T. Below around 75–70 K we could not measure the resistance of this sample since it was above the PPMS internal resistance. The data are plotted in the adequate scales (log R vs $1/T$) so that the slopes of the straight regions evidence the changes in the activation energy E_A [$R=R_0 \exp(E_A/k_BT)$].[29]

At high temperatures the activation energy E_A is identical for both directions (135 meV). The anisotropy clearly arises around T_C where the ferromagnetic phase is established and the activation energy decreases. The values of E_A, and of the normalized resistance, are now different depending on the direction of the current even without an external magnetic field. The higher value corresponds to the current parallel to the growth axis that we labeled as the AF axis [$E_A(\parallel)=57$ meV and $E_A(\perp)=43$ meV]. In the range between T_C and T_{OO} the reported resistivity behavior of nominally identical compounds varies in the literature. Sometimes a metallic behavior ($dR/dT>0$) is reported.[15] This again evidences the consequence of small departures from the nominal composition around $x=0.1$. The standard negative MR in manganites is found around T_C in both directions but, below T_{C2}, for $I \perp$ ga (along the easy ferromagnetic direction) a positive magnetoresistance (higher resistance with applied

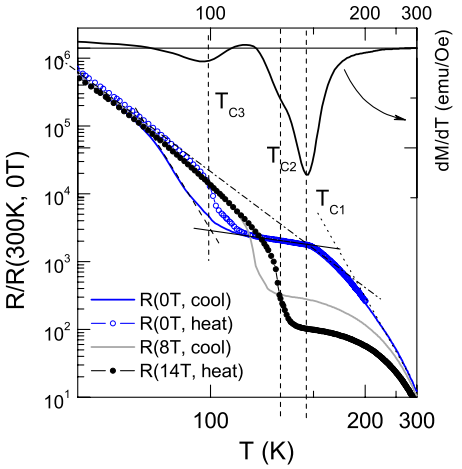

FIG. 7. (Color online) Resistance of sample B as a function of temperature for $H=0$, 8, and 14 T. The comparison with the susceptibility derivative shows their correlations. (Note the reciprocal scale used for the temperature.)

field) and a hysteresis between cooling and heating are observed [Fig. 6(b)].

Figure 7 plots the temperature dependence of the resistance and of the susceptibility derivative $d\chi/dT$ of sample B with $T_{OO}=97$ K. The higher value of T_{OO} allows observing the increase in E_A when the orbital order is established. At high temperatures ($T>220$ K) $E_A=170$ meV but, contrary to sample A, the resistivity deviates from the activated behavior at around 220 K due to short-range ferromagnetic correlations observed in this sample above T_C. In the $T_C>T>T_{OO}$ range, the activation energy is reduced to $E_A=16$ meV and it increases below T_{OO} to $E_A=72$ meV. The important hysteresis in $R(T)$ curves between cooling and heating both at 0 T indicates that the orbital-order (OO) transition is of first order. It is important to note that the activation energy in this phase is lower than that of the paramagnetic phase. Since the polaron trapping energy is related to the cooperative JT distortion of MnO octahedra[30] the close value of E_A in the $T_C<T<T_{JT}$ ($\approx$340 K) range confirms that these distortions are similar to those in $LaMnO_3$. The important diminution of E_A in the low-temperature orbital-ordered ferromagnetic phase ($E_A=72$ meV) is an indication of the reduction of the JT distortions compared to those in the orbital-ordered high-temperature phase.[7]

At T_{OO} the orbital order is accompanied by a rearrangement of the magnetic structure which can be induced by an external magnetic field.[15] Looking in detail to the temperature range between T_C and T_{OO}, we observe this metamagnetic hysteretic transition in the magnetic cycles at temperatures below the AF ordering as an increase of the saturation magnetization. The effects on the resistivity [Fig. 7, $R(T)$ at 8 and 14 T] and on the magnetoresistance (Fig. 8) indicate that the high-resistivity regime of the OO order is reached at higher temperatures with external applied magnetic fields. The usual negative MR is observed, with the largest values around T_C [continuous lines in Fig. 8(a)] and small values at low temperatures (8% at 8 T and 80 K), as it corresponds to a single crystal. But, in the temperature range between T_{C2} and T_{OO}, the steep increase in resistance [curves with symbols in Fig. 8(a)] is due to the field induced magnetic and OO transition. The hysteretic behavior is a signature of the first-order character of the transition and is also responsible for the difference in the measured resistance upon cooling and heating ($H=0$ T) in Fig. 7. Therefore a stronger ferromagnetic phase is concomitant with a higher resistive phase. The inset of Fig. 8 shows the evolution with temperature of the field necessary to promote the OO phase in the temperature range $T_{OO}<T<T_{C2}$.

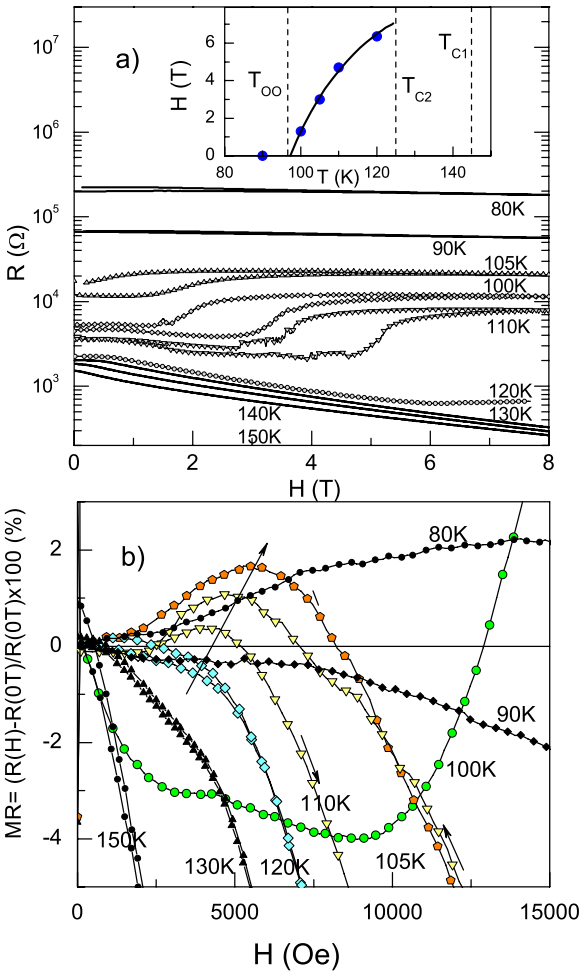

FIG. 8. (Color online) (a) Resistance vs applied magnetic field up to 8 T of sample B with $T_C=143$ K, $T_{C2}=125$ K, and $T_{OO}=97$ K. Data represented with symbols correspond to temperatures between T_{C2} and T_{OO}. Inset: Magnetic field necessary to induce the high-resistivity regime vs temperature. (b) Low-field MR. Colored symbols correspond to temperatures between T_{C2} and T_{OO}.

Looking at the low-field magnetoresistance (LFMR) [Fig. 8(b)], i.e., below 1 T, small but noteworthy effects are observed. At 145 K the MR is due to the reduction of the carrier scattering by spin disorder. Below T_C, the LFMR is considerably reduced and, between T_{C2} and T_{OO}, it is positive for low fields, negative for intermediate fields, and finally positive when the OO is established. Therefore, besides the huge positive MR at high fields related to the induced OO phase [Fig. 8(a)], a small positive MR is observed for fields around 5000 Oe for $T_{C2}>T>T_{OO}$. This can be explained by the magnetic anisotropy and AF correlations. The

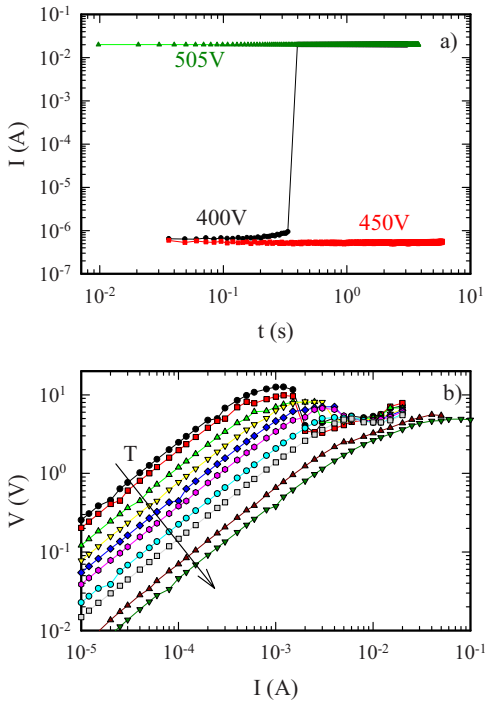

FIG. 9. (Color online) (a) Time dependence of current after application of dc voltage, $T=20$ K. (b) Four-contact dc I-V curves at temperatures (from above) $T=78$, 80, 85, 90, 95, 100, 110, 120, 140, and 150 K.

applied field increases the spin disorder in the structural domains when its direction coincides with AF axes (a and/or b) of the domain, increasing the overall measured resistance. Once this disorder is overcome, the resistivity decreases down to the field at which the OO order is induced and then increases again.

C. Electroresistance

ER measurements have been obtained in the untwinned A crystal for different directions of the current. Discontinuous high resistive (HR) $\rightarrow$ low resistive (LR) transitions at $T>70$ K, when $R\leq 50$ kΩ, have been detected in four-contact configuration. At lower temperatures, when the resistance is too high to be measured in four-point configuration, two contact measurements were used with a fixed applied voltage and measuring current. It is known that I-V measurements in manganites are always affected by Joule heating, especially at low temperatures when the specific heat of the sample is small. This is why we took special care in discarding heating effects by measuring the I-V characteristics at very short times after the voltage or current was applied, before heating masks the intrinsic ER, by applying low-current densities and by checking the results with samples directly immersed into liquid nitrogen.

Two types of low-temperature measurements are shown in Fig. 9. At $T=20$ K, a constant voltage is applied at $t=0$ s and the current is measured as a function of time. In such a measurement, Joule heating would increase the current (resistance decrease) continuously. It is clear that in the time frame of milliseconds to seconds no heating is observed. For $V<400-450$ V (with $I<1$ μA), the sample is in the HR state ($R_{2c}=5.7\times 10^8$ Ω) and for voltages higher than a critical value ($V>500$ V), in the LR state. If the current exceeds approximately 1 μA, there is an abrupt switch into a low resistive state. Usually, this switch is immediate, i.e., upon applying voltage current has immediately either HR or LR values (traces $V=450$, 505 V in Fig. 9). In very few occasions, this switch is observed in the time frame of our experiment (as 400 V trace in Fig. 9). The immediate jump of current, and therefore of resistance, is very large (more than 4 orders of magnitude) and the current hits the instruments current compliance limit (20 mA in this case). Note that $V=505$ V trace is also cut at the current compliance limit; thus, from this experiment we can just deduce the upper limit of the LR value. Subsequent measurements at $V=450$ V lacked to induce the LR state. This shows that (i) HR $\rightarrow$ LR transitions are not caused by heating and (ii) there is a voltage region where the sample can be either in the HR or LR state evidencing the first-order nature of this effect.[24] The lower panel of Fig. 9 shows four-contact I-V curves for $I\perp$ ga (we will call this direction "a_1") at temperatures $78<T<150$ K. For currents below $I=1$ mA the ohmic behavior is evident, while sharp drops [negative differential resistance (NDR)] are observed for $1<I<10$ mA up to around 120 K. The threshold current I_t of this drop increases with temperature and disappears at T_{C2}. Note that the $V(I)$ curve at $I>I_t$ restores its positive slope ($dV/dI>0$) indicating that the sample has entered into a different resistive state.

It is important to note that the abrupt jump of voltage reported in polycrystalline $Nd_{0.5}Ca_{0.5}Mn_{0.96}Cr_{0.04}O_3$, which was associated to an increase in the temperature of the sample, is due to the drastic change of conductivity through the temperature induced insulating to metallic phase transition.[19] In the present case, the crystals are always insulating, therefore the discontinuous transitions cannot be related to this Joule heating effects.

Having in mind the observed magnetic and transport anisotropies, we have measured the ER along three different directions of the current. Figure 10 shows the I-V curves for sample A immersed into liquid nitrogen ($T=77$ K). In Fig. 10(a) the measurements were done along two mutually perpendicular directions in the plane of the disk, therefore perpendicular to the ga. We labeled these two directions as "a_1" and "a_3." These two directions are equivalent from the geometrical side, so the resistance values can be directly compared. The obtained low-current resistances ($I<0.5$ mA) along these two directions are identical. However, one can see a clear anisotropy in their dependence on the applied voltage. For $I\|a_1$ a sharp voltage drop (HR to LR) occurs at $I_t=0.5$ mA (see inset) and for larger currents the sample has entered into a different resistive regime: $dV/dI=30$ kΩ and 50 Ω for HR and LR, respectively. The I-V curve is completely different along the a_3 direction. The HR regime gives the same resistance of 30 kΩ, but no discontinuous transition is observed. At $I>4$ mA, a NDR with subsequent minor transitions are present.

Although it is not possible to definitely rule out that the NDR at high currents in the a_3 direction is not a consequence of local heating, the comparison of a_1 and a_3 current directions ensures that at least the I-V curve in a_1 the direction is

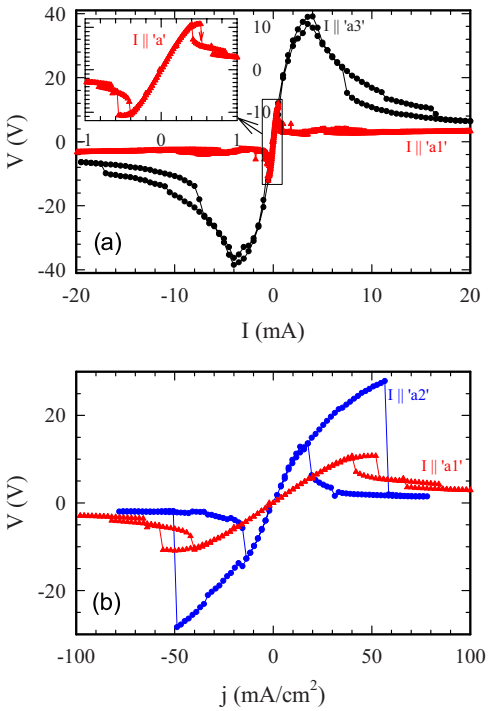

FIG. 10. (Color online) *I-V* curves for sample A along different current directions at $T=77$ K (sample into liquid nitrogen). (a) Two perpendicular directions in the plane of the disk perpendicular to the ga; a_1 (red triangles) and a_3 (black points). Inset shows a zoom of $I \| a_1$ for low current. (b) Voltage vs current density j_t for current $I \| a_1$ (red triangles) and $I \| a_2 \| ga$ (blue diamonds).

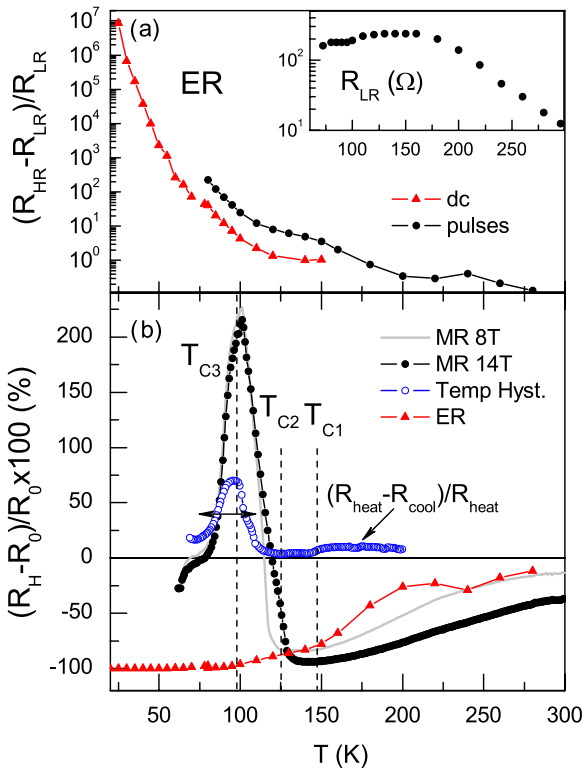

FIG. 11. (Color online) (a) Temperature dependence of ER $=(R_{HR}-R_{LR})/R_{LR}$. Diamonds: dc measurements, triangles: high-temperature pulsed measurements. Inset: Resistance of the current induced low resistive state vs temperature. (b) Comparison of the MR and ER in the standard definition for sample B. Open dots correspond to the hysteresis between heating and cooling without magnetic field.

not caused by heating: the same incoming power $P=IV$ is not yielding the same heating effect. Figure 10(b) shows the third direction, called "a_2," when current flows along the crystal ga. In order to compare the same effect for two different geometrical arrangements, the voltage is plotted as a function of the current density **j**. The larger effect, HR to LR drop, is detected along this direction, which also shows the higher resistivity. But the threshold current density j_t is approximately equal for $I \| a_2$ and $I \| a_1$; thus, it appears that these two directions are almost equivalent. On the contrary, when $I \| a_3$ it is much more difficult to achieve the ER drop $[I_t(a_3) > 8 I_t(a_1)]$.

The temperature dependence of the resistance in the current induced low resistive state R_{LR} has been obtained either by pulsed, down to around 70 K, or dc measurements. With these values we can obtain the ER factor which is up to 10^7 [Fig. 11(a)]. The ER has been plotted using the "inflated" definition where the difference is divided by the small resistance R_{LR}. This definition is necessary to evidence such colossal resistivity changes when the standard definition saturates at 100%. The pulsed measurements are much more efficient to avoid heating problems but are not accessible at the lowest temperatures. Nevertheless, the reliability of ER obtained from dc values is proven from the reasonable coincidence with ER values using pulses in the whole region where both data have been recorded (70–150 K). Below T_C down to the lowest measured temperature (20 K) the low resistive state shows a metallic-type conduction[24] which is induced by current densities as low as 10^{-8} A/cm^2 at 20 K.

Finally we will compare the effects of external magnetic and electric fields on the conductivity.

The effect of an applied magnetic field on the resistivity is similar to that of current for temperatures above T_{C2} [Fig. 11(b)]; in fact, ER values coincide quantitatively with MR at 8 T. On the contrary, magnetic and electric fields produce opposite effects at lower temperatures. The positive MR, which peaks around T_{OO}, is due to the magnetic field induced orbital-order transition that increases the resistivity of the sample. Also, the hysteresis in temperature of the OO transition originates the blue dotted curve in Fig. 11. On the contrary, the colossal values of ER are obtained by overcoming the orbital order and allowing a metallic conductivity.

The differences in the transition temperatures reported in the literature for $x=0.1$ compounds are related to subtle differences in the actual composition that, at this phase diagram boundary, give rise to differences in the crystalline, electronic, and magnetic phases. T_{JT} and T_{OO} are the most sensitive to composition or to the formation of chemically inhomogeneous phases. Even the samples presented here, with identical T_C and T_{C2}, show different T_{JT} (342 and 335 K) and T_{OO} (73 and 97 K). We propose the phase diagram of Fig. 1(b) for a close region around $x=0.1$, where the composition of sample B is shifted to $x=0.103$ following the linear behaviors of decreasing T_{JT} and increasing T_{OO} with x. Therefore, the sample with the lowest T_{OO} (sample A) would be

closer to the diagram phase boundary converging toward $T_{OO}=0$ since on the left side of the phase diagram this transition disappears. It is almost impossible to fix the composition of the samples within the required accuracy; therefore samples A and B are not identical as neither is reported in previous works. $T_{OO}=73$ K is the lowest temperature reported for $La_{1-x}Sr_xMnO_3$ and sample A shows characteristics of both sides of the phase diagram.

IV. CONCLUSIONS

A magnetic and transport study of several twinned and untwinned $La_{0.9}Sr_{0.1}MnO_3$ single crystals allowed us to observe strong magnetocrystalline anisotropy as well as anisotropy in conductivity and electroresistance. At $T_C=143$ K an incomplete long-range ferromagnetic order is established; ac susceptibility shows some characteristics of spin-glass-like behavior indicating that magnetic frustration occurs due to AF correlations. At $T_{C2}=125$ K the AF correlations order, leading to the magnetic anisotropy which is related to the observation of different activation energies for conductivity depending on the current direction even without applied magnetic field. The orbital-order phase (at $T_{OO}=73$ to 97 K depending on the ingot) induces another magnetic reorganization which maintains the anisotropy. At T_{OO} the activation energy for conduction increases but is, in fact, considerably smaller than in the paramagnetic phase. Quite low-current densities are able to induce a metallic behavior that may be associated to the destruction of the orbital lattice polaron or orbital order. An interesting experiment would be to check if the sample, in the current induced low resistive state, shows a magnetization increase up to the full collinear ferromagnetic value. Below T_{C2}, the observed anisotropies of magnetism and electronic transport are rather contrary to phase segregation or spin-glass-like situations. The insulating character below T_C indicates that the double exchange ferromagnetic correlations are not enough to overcome the strong electron-phonon coupling and superexchange antiferromagnetic correlations. Nevertheless, it produces a lowering of the trapping energy of the polarons. Below T_{OO} the orbital order could be similar to the proposed for $x=0.125$ (Ref. 11) which presents a clear anisotropy between *ab* planes and the *c* axis. The reports from samples with nominal composition $x=0.1$ present diverse behaviors due to the drastic effects of small composition deviations whose strongest indicators are the structural and orbital-order transitions (T_{JT} or T_{OO}). Using the tendencies of these transition temperatures with x and the here-presented data, we propose a phase diagram around $x=0.1$. The crystal with the lowest T_{OO} corresponds to the composition closest to the vertical phase diagram boundary and presents phases characteristic of both sides of the boundary. The canted AF phase that appears in between T_C and T_{OO} is responsible for the magnetic and transport anisotropies that persist down to 5 K.

ACKNOWLEDGMENTS

We acknowledge financial support from the Spanish Ministerio de Educación y Ciencia under Contracts No. MAT2005-06024-CO2-01 and No. MAT2006-01004 and Ramón y Cajal program (N.B.).

*ada@icmm.csic.es

[1] For an overview on manganites, see, for example, E. Dagotto, T. Hotta, and A. Moreo, Phys. Rep. **344**, 1 (2001).
[2] G. L. Liu, J. S. Zhou, and J. B. Goodenough, Phys. Rev. B **64**, 144414 (2001).
[3] K. Mukherjee and A. Banerjee, Phys. Rev. B **77**, 024430 (2008).
[4] E. Rozenberg, M. Auslender, A. I. Shames, G. Gorodetsky, and Ya. M. Mukovskii, Appl. Phys. Lett. **92**, 222506 (2008).
[5] J. Deisenhofer, D. Braak, H. A. Krug von Nidda, J. Hemberger, R. M. Eremina, V. A. Ivanshin, A. M. Balbashov, G. Jug, A. Loidl, T. Kimura, and Y. Tokura, Phys. Rev. Lett. **95**, 257202 (2005).
[6] V. Skumryev, J. Nogues, J. S. Munoz, B. Martinez, R. Senis, J. Fontcuberta, L. Pinsard, A. Revcolevschi, and Y. M. Mukovskii, Phys. Rev. B **62**, 3879 (2000).
[7] J. Geck, P. Wochner, S. Kiele, R. Klingeler, P. Reutler, A. Revcolevschi, and B. Büchner, Phys. Rev. Lett. **95**, 236401 (2005).
[8] S. S. Grenier, K. J. Thomas, J. P. Hill, U. Staub, Y. Bodenthin, M. García-Fernández, V. Scagnoli, V. Kiryukhin, S.-W. Cheong, B. G. Kim, and J. M. Tonnerre, Phys. Rev. Lett. **99**, 206403 (2007).
[9] D. E. Cox, T. Iglesias, E. Moshopoulou, K. Hirota, K. Takahashi, and Y. Endoh, Phys. Rev. B **64**, 024431 (2001).
[10] J. Geck, P. Wochner, D. Bruns, B. Büchner, U. Gebhardt, S. Kiele, P. Reutler, and A. Revcolevschi, Phys. Rev. B **69**, 104413 (2004).
[11] Y. Endoh, K. Hirota, S. Ishihara, S. Okamoto, Y. Murakami, A. Nishizawa, T. Fukuda, H. Kimura, H. Nojiri, K. Kaneko, and S. Maekawa, Phys. Rev. Lett. **82**, 4328 (1999).
[12] G. Papavassiliou, M. Pissas, G. Diamantopoulos, M. Belesi, M. Fardis, D. Stamopoulos, A. G. Kontos, M. Hennion, J. Dolinsek, J.-Ph. Ansermet, and C. Dimitropoulos, Phys. Rev. Lett. **96**, 097201 (2006).
[13] H. Kawano, R. Kajimoto, M. Kubota, and H. Yoshizawa, Phys. Rev. B **53**, 2202 (1996).
[14] K. Ghosh, R. L. Greene, S. E. Lofland, S. M. Bhagat, S. G. Karabashev, D. A. Shulyatev, A. A. Arsenov, and Y. Mukovskii, Phys. Rev. B **58**, 8206 (1998).
[15] R. Senis, V. Laukhin, B. Martinez, J. Fontcuberta, X. Obradors, A. A. Arsenov, and Y. M. Mukovskii, Phys. Rev. B **57**, 14680 (1998).
[16] A. Asamitsu, Y. Tomioka, H. Kuwahara, and Y. Tokura, Nature (London) **388**, 50 (1997); M. Fiebig, K. Miyano, Y. Tomioka, and Y. Tokura, Science **280**, 1925 (1998).
[17] M. Tokunaga, Y. Tokunaga, and T. Tamegai, Phys. Rev. Lett. **93**, 037203 (2004).
[18] J. Sacanell, A. G. Leyva, and P. Levy, J. Appl. Phys. **98**, 113708 (2005).
[19] A. S. Carneiro, R. F. Jardim, and F. C. Fonseca, Phys. Rev. B **73**, 012410 (2006).

[20] S. Mercone, R. Frésard, V. Caignaert, C. Martin, D. Saurel, G. André, P. Monod, and F. Fauth, J. Appl. Phys. **98**, 023911 (2005).
[21] A. de Andrés, M. García-Hernández, and J. L. Martínez, Phys. Rev. B **60**, 7328 (1999).
[22] C. Barone, C. Adamo, A. Galdi, P. Orgiani, A. Yu. Petrov, O. Quaranta, L. Maritato, and S. Pagano, Phys. Rev. B **75**, 174431 (2007).
[23] V. Markovich, E. Rozenberg, Y. Yuzhelevski, G. Jung, G. Gorodetsky, D. A. Shulyatev, and Ya. M. Mukovskii, Appl. Phys. Lett. **78**, 3499 (2001).
[24] N. Biškup, A. de Andrés, N. M. Nemes, M. García-Hernandez, K. V. Glazyrin, and Y. M. Mukovskii, Appl. Phys. Lett. **90**, 222502 (2007).
[25] H. Jain, A. K. Raychaudhuri, Nilotpal Ghosh, and H. L. Bhat, Phys. Rev. B **76**, 104408 (2007).
[26] N. Biškup and A. de Andrés, Phys. Rev. B **74**, 184403 (2006).
[27] D. Shulyatev, S. Karabashev, A. Arsenov, Ya. Mukovskii, and S. Zverkov, J. Cryst. Growth **237-239**, 810 (2002).
[28] The calculations of the demagnetization factors (N) for cylinders are complicated. A very rough approximation would use the N factors of a thin film that represents the extreme situation with $L \ll D$. In this case $N=0$ for $H \parallel$ film plane ($H \perp$ ga) and $N=1$ for $H \perp$ film plane ($H \parallel$ ga). Consequently, while in the geometry with $H \perp$ ga the demagnetization effect is small; with $H \parallel$ ga it reduces substantially the effective field.
[29] The formula for an activated conduction instead of that for a polaron mechanism is used because of its simplicity for graphical representation and because, in such narrow temperature ranges, the differences between them are insignificant.
[30] L. Martín-Carrón, A. de Andrés, M. J. Martínez-Lope, M. T. Casais, and J. A. Alonso, Phys. Rev. B **66**, 174303 (2002).